Symmetry analysis of the localized modes associated with substitutional and interstitial defects in a two-dimensional triangular photonic crystal

Vladimir Kuzmiak* and Alexei A. Maradudin
Department of Physics and Astronomy, University of California, Irvine, California 92697
(Received 21 July 1999)

By using a finite-difference time-domain numerical method based on the numerical simulation of the excitation of an isolated eigenstate at a specific frequency by using an oscillating dipole embedded in a two-dimensional photonic crystal we have calculated both the eigenfrequencies and eigenfunctions of the localized defect modes induced by defect cylinders placed at the center or in interstitial positions within an otherwise perfect two-dimensional photonic crystal consisting of dielectric cylinders arrayed in a triangular lattice. In the case of a substitutional defect cylinder we have imposed boundary conditions appropriate to the irreducible representations of the C_{6v} point group, and in addition to fully symmetric localized states of A_1 symmetry we have also found localized modes possessing A_2, B_1, and B_2 symmetry, and doubly degenerate modes of E_1 and E_2 symmetry. For defect rods placed in interstitial positions we have found localized modes that belong to the irreducible representations A_1, A_2, B_1, and B_2 of the C_{2v} point group. We have also studied the effects of the geometrical and material parameters on the eigenfrequencies and eigenfunctions of the defect modes by varying the dielectric strength and/or radius of the defect rods. We have shown that the calculated eigenfrequencies obtained for a substitutional defect rod within the triangular lattice with lattice constant a whose radius r_d is in the interval $0<r_d<0.5a$ are in good quantitative agreement with both the nondegenerate and degenerate modes obtained by the supercell method by Feng and Arakawa [Jpn. J. Appl. Phys. Part 2 **36**, 120(1997)].

I. INTRODUCTION

The concept of the photonic crystal introduced a decade ago[1,2] attracted a great deal of interest and stimulated intensive research into photonic-band-gap (PBG) materials[3,4] that exhibit full photonic band gaps in which electromagnetic waves of both polarizations are forbidden to propagate. The existence of a photonic band gap gives rise to a number of interesting phenomena, such as an inhibition of spontaneous emission, which can be utilized in improving the behavior of many optical and electronic devices such as semiconductor lasers, solar cells, and bipolar transistors.[1,2]

In analogy to the existence of the defect states within the energy band gaps in semiconductors, in photonic crystals exponentially decaying localized defect modes may appear within a photonic band gap when a defect is introduced into an otherwise perfect photonic crystal.[1,5–21] The nature of the localized modes has been under intensive theoretical and experimental study, in particular in view of their potential applications in semiconductor lasers, resonators, single-mode emitting diodes, etc. The localized modes in a PBG structure have, as do ordinary high-Q resonators, the ability to control spontaneous emission. However, in contrast to their counterparts in quantum electrodynamic (QED) cavities, PBG modes can extend spatially over many wavelengths. In addition to the fact that through the PBG localized modes spontaneous emission is inhibited, these defect modes also facilitate coherent energy transport,[22] and can modify other physical phenomena as a consequence of their unique properties.

The calculations of the frequencies and the fields associated with these defect modes were initially performed by using supercell and transfer-matrix methods.[8,10–13,16,17] Later, a number of methods based on the application of the Green's-function formalism[11,14,15,18] and real space finite-difference time-domain (FDTD) methods[20,23,24] were reported. These numerical techniques that allow studying the interaction of the electromagnetic radiation with more complex structures proved to be efficient tools for accurately calculating defect modes.[16,17,25] By employing the ideas behind FDTD numerical methods designed to obtain the dispersion relations of phonons and photons in disordered systems[26,27] there was developed an approach based on the numerical simulation of the excitation of a single mode by using an oscillating dipole moment located near a dielectric defect.[28] This method has been applied to the study of the defect modes in photonic crystals consisting of infinitely long parallel dielectric rods arranged in simple square and triangular lattices,[29,30] and of line defects.[31]

In this paper we study the symmetry and the field patterns of the defect modes that appear within the band gaps of a triangular photonic crystal when an impurity rod is placed either in simple substitutional or interstitial positions within the supercell, and the dependence of the eigenfrequencies on the dielectric constant and/or radius of the defect rod. To determine the eigenfrequencies and eigenfunctions of the localized modes we apply a finite-difference time-domain technique developed within a Green's-function approach[28] applied to a defect problem.[29] The method is based on the numerical simulation of the excitation of the defect mode by a virtual oscillating dipole located near the dielectric defect. In the first step, by solving the inhomogeneous wave equation discretized in both space and time, the electric field radiated from the oscillating dipole is determined. Then the electromagnetic energy emitted by the dipole as a function of

frequency is evaluated, and the frequency of the defect mode is determined as a resonance frequency. The systematic study of the localized modes in two-dimensional (2D) structures provides valuable information that can be used in the design of photonic band-gap structures and devices operating in the near infared and optical regimes in which high-Q resonant cavities are used. The growing interest in two-dimensional structures stems from the fact that they are easier to fabricate than three-dimensional structures, and also provide broader ranges of geometrical and material parameters for which localized defect modes within the photonic band gaps exist.

In Sec. II we describe the theoretical background for the numerical simulations used in calculating the eigenfrequencies and the eigenfunctions of the defect modes. In Sec. III we present results for the localized modes associated with a defect cylinder placed in substitutional and interstitial positions within a triangular lattice, which corresponds to the system studied experimentally in Ref. 12, and identify the localized modes belonging to substitutional and interstitial defects in terms of the symmetries corresponding to the irreducible representations of the point groups C_{6v} and C_{2v}, respectively. We study the variation of the defect levels that appear in the photonic band gaps when the dielectric constant and/or the radius of the defect cylinder(s) is modified. In Sec. IV we summarize and discuss the results.

II. METHOD OF CALCULATION

We consider a two-dimensional photonic crystal that consists of infinitely long parallel rods characterized by a dielectric constant ϵ_a embedded in a background dielectric material characterized by the dielectric constant ϵ_b. The rods are assumed to be parallel to the x_3 axis, and the intersections of the axes of the rods with a perpendicular plane form a two-dimensional triangular lattice. In particular, we are interested in exploring the nature of defect modes of C_{6v} and C_{2v} symmetry that appear within a photonic band gap when a defect cylinder with modified radius and/or dielectric constant is introduced into the otherwise perfect two-dimensional photonic crystal.

For the vector electromagnetic field in a 2D photonic lattice the Maxwell equations decouple into separate equations for E-polarized (TM) and H-polarized (TE) modes, with the electric field and magnetic field parallel to the rod axis, respectively.[5,32,33] The two-dimensional system we study is characterized by a dielectric constant of the form

$$\epsilon(\mathbf{x}_\parallel)=\epsilon_0(\mathbf{x}_\parallel)+\epsilon_d(\mathbf{x}_\parallel), \tag{2.1}$$

where $\epsilon_0(\mathbf{x}_\parallel)$ is a periodic function of $\mathbf{x}_\parallel$,

$$\epsilon_0[\mathbf{x}_\parallel+\mathbf{x}_\parallel(l)]=\epsilon_0(\mathbf{x}_\parallel), \tag{2.2}$$

with $\mathbf{x}_\parallel(l)$ a translation vector of the triangular lattice, while $\epsilon_d(\mathbf{x}_\parallel)$ is nonzero in only a small region of the x_1x_2 plane.

In this paper we will consider the particular case of the defect states of E polarization with the electric vector given by

$$E(\mathbf{x};t)=(0,0,E_3(\mathbf{x}_\parallel;t)), \tag{2.3}$$

and

$$H(\mathbf{x};t)=(H_1(\mathbf{x}_\parallel;t),H_2(\mathbf{x}_\parallel;t),0). \tag{2.4}$$

To calculate the eigenfrequencies and the eigenvectors of the defect modes in a triangular lattice we employ an approach based on the application of the Green's-function formalism,[28] which describes the radiation from an oscillating dipole in an arbitrary 3D lattice,[28] applied to the defect problem.[29] In order to excite an isolated eigenstate selectively, a narrow source in the form of an oscillating dipole is placed at an appropriate point within a computational cell. We assume that the direction of the dipole moment $\mathbf{d}_\mu$ of frequency ω centered at (x_{10},x_{20}) within the x_1x_2 plane is parallel to the rods, so that Maxwell's equations for the amplitude functions $E_3(\mathbf{x}_\parallel;t)$, $H_1(\mathbf{x}_\parallel;t)$, and $H_2(\mathbf{x}_\parallel;t)$ become

$$\frac{\partial E_3}{\partial x_1}=\frac{1}{c}\frac{\partial}{\partial t}H_2, \tag{2.5}$$

$$\frac{\partial E_3}{\partial x_2}=-\frac{1}{c}\frac{\partial}{\partial t}H_1, \tag{2.6}$$

$$\frac{\partial H_2}{\partial x_1}-\frac{\partial H_1}{\partial x_2}=\frac{1}{c}\frac{\partial}{\partial t}\{\epsilon(\mathbf{x}_\parallel)E_3+4\pi d_\mu \times\delta(x_1-x_{10})\,\delta(x_2-x_{20})\exp(-i\omega t)\}. \tag{2.7}$$

By eliminating H_1 and H_2 the equation for E_3 can be written in the form

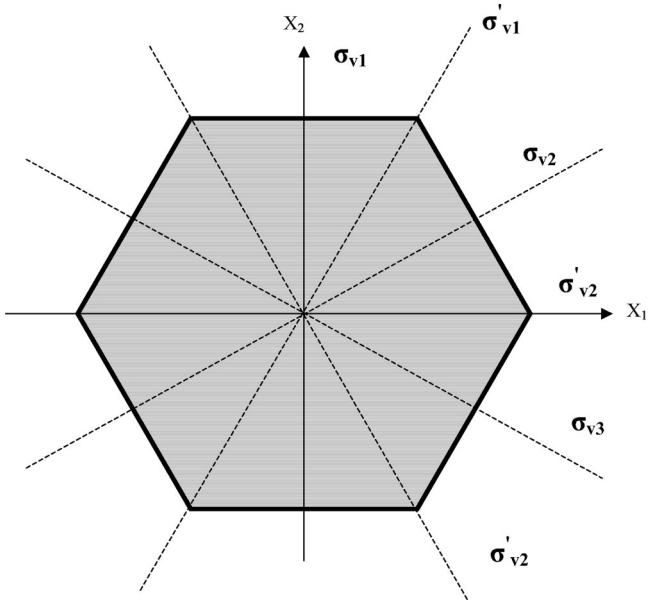

FIG. 1. The computational domain in the x_1x_2 plane assumed in the numerical calculations that consists of rods with ϵ_a arrayed in a lattice characterized by the lattice constant a embedded in a background medium with ϵ_b and an isolated substitutional defect characterized by ϵ_d placed in the center of the domain.

$$\frac{\epsilon(\mathbf{x}_\parallel)}{c^2}\frac{\partial^2}{\partial t^2}E_3=\left(\frac{\partial^2}{\partial x_1^2}+\frac{\partial^2}{\partial x_2^2}\right)E_3-\frac{\omega^2}{c^2}4\pi d_\mu \times\delta(x_1-x_{10})\,\delta(x_2-x_{20})\exp(-i\omega t). \tag{2.8}$$

Then by approximating the spatial and time derivatives in the latter equation by finite differences, one obtains

$$E_{i,j}^{k+1}=2E_{i,j}^{k}-E_{i,j}^{k-1}+\frac{1}{\epsilon_{i,j}}\left(\frac{\Delta t}{\Delta x_1}\right)^2[E_{i+1,j}^{k}+E_{i-1,j}^{k}-2E_{i,j}^{k}] +\frac{1}{\epsilon_{i,j}}\left(\frac{\Delta t}{\Delta x_2}\right)^2[E_{i,j+1}^{k}+E_{i,j-1}^{k}-2E_{i,j}^{k}] +\frac{4\pi d_\mu}{\epsilon_{i,j}}(\omega\Delta t)^2\frac{\delta_{ii0}}{\Delta x_1}\frac{\delta_{jj0}}{\Delta x_2}\exp(-i\omega kt), \tag{2.9}$$

where the index k refers to a grid point of time, the indices i and j denote the x_1 and x_2 axes, respectively, Δt is the division of time, and Δx_1, Δx_2 are the intervals between the neighboring nodes along the x_1 and x_2 axes, respectively, on a discrete two-dimensional mesh. To evaluate the electric field radiated from the oscillating dipole we solve Eq. (2.9) with the initial conditions $E_3(\mathbf{x}_\parallel;0)=0$, $\partial E_3(\mathbf{x}_\parallel;0)/\partial t=0$.

By using the values of the electric field obtained by solving Eq. (2.9) in a computational domain we determine the components of the magnetic field to evaluate the electromagnetic energy U emitted per unit time by the oscillating dipole placed at $\mathbf{x}_0$ within the supercell. It is given by the surface integral of the normal component of the Poynting vector, which can be transformed into a volume integral by using Gauss's theorem. By calculating the Poynting vector and by using the normalization condition

$$\int_V \epsilon(\mathbf{x})|\mathbf{E}_d(\mathbf{x})|^2 d\mathbf{x}=V, \tag{2.10}$$

where $\mathbf{E}_d(\mathbf{x})$ is the eigenfunction of the defect mode and V is the volume on which the cyclic boundary conditions are applied, one obtains

$$U=\frac{\pi\omega_d^2|\mathbf{d}_\mu\cdot\mathbf{E}_d(\mathbf{x}_0)|^2}{2V\{(\omega-\omega_d)^2+\Gamma^2\}}. \tag{2.11}$$

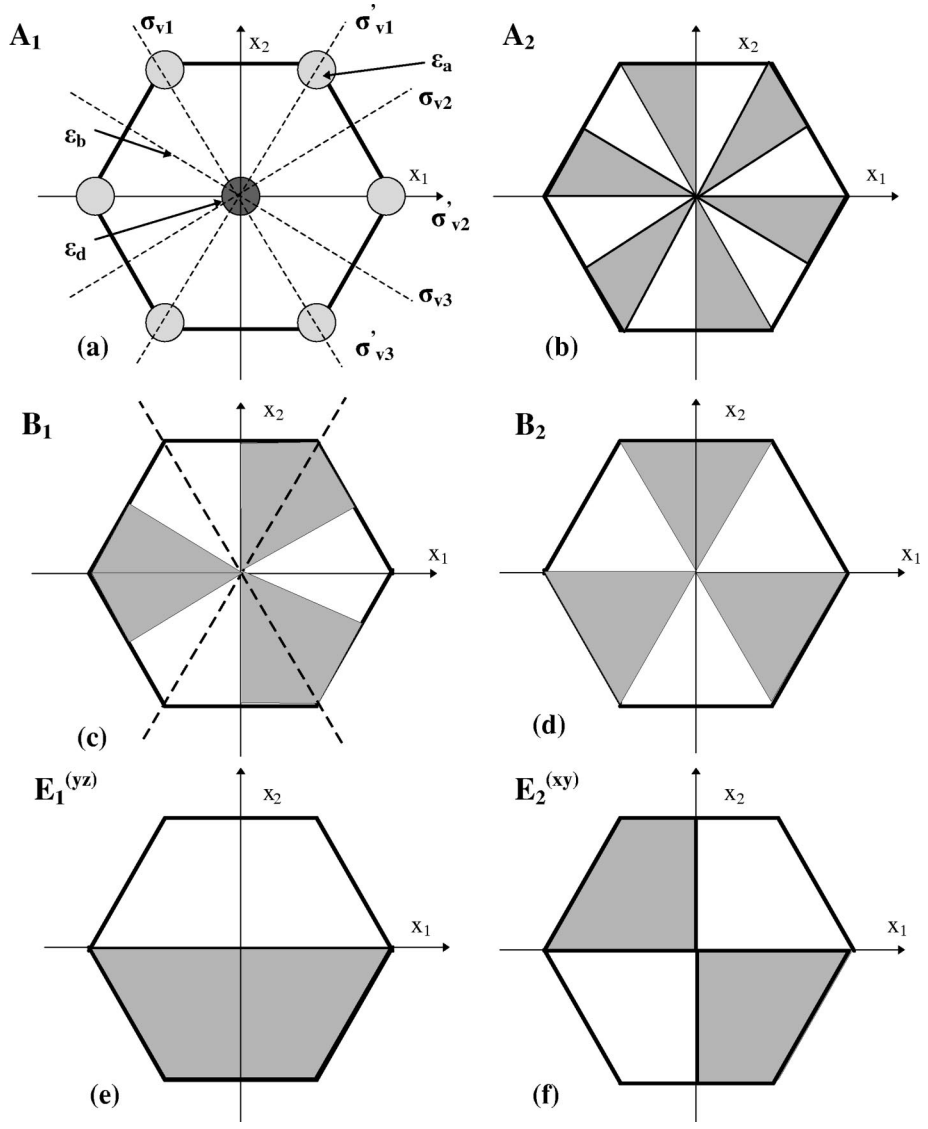

FIG. 2. The central part of the computational domain consisting of the six nearest neighbors in the vicinity of a simple substitutional defect rod placed in the center in the supercell (a) and symmetry patterns that belong to all possible irreducible representations of the point group C_{6v}. Shaded and blank areas indicate the subdomains that are symmetric and asymmetric with respect the symmetry operations applied to the irreducible subdomain represented by 1/12 and 1/4 of the supercell [(b)–(f)].

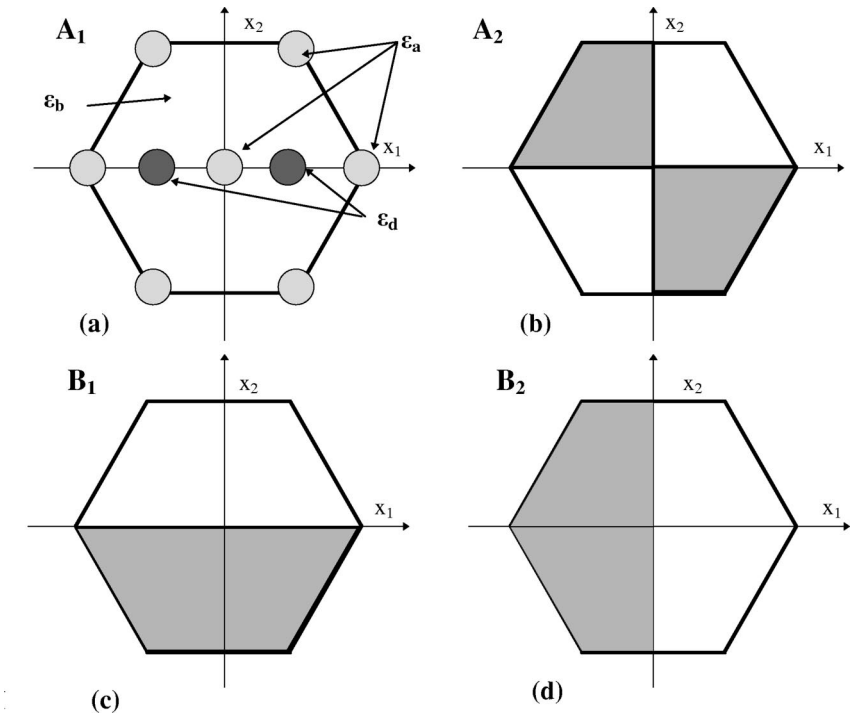

FIG. 3. The central part of the computational domain used for the calculation of the defect consisting of two interstitial defect rods placed along the [1,0] direction (a) and symmetry patterns that belong to all possible irreducible representations of the point group C_{2v}. Shaded and blank areas indicate the subdomains that are symmetric and asymmetric with respect to the symmetry operations applied to the irreducible subdomain represented by 1/4 of the supercell.

Here Γ is a small positive constant that ensures the causality of the Maxwell curl equations for the electric and magnetic fields given by Eqs. (2.5)–(2.7). From the frequency dependence of the electromagnetic energy emitted by the dipole per unit time given by Eq. (2.11) we determine the frequency of the defect mode as the resonance frequency.

The difference equation (2.9) is solved numerically in the x_1x_2 plane within a computational domain shown in Fig. 1 consisting of 8×8 unit cells, each of which is characterized by the lattice constant a. Each unit cell is sampled on a 40×40 mesh, and we take 320 time steps per oscillation period. We found that by using these steps of spatial and temporal discretization the eigenfrequencies and eigenfunctions of the localized modes are converged with an error that is smaller than 1%. The fields at the nodes outside the computational domain are related to the fields inside it by impos-

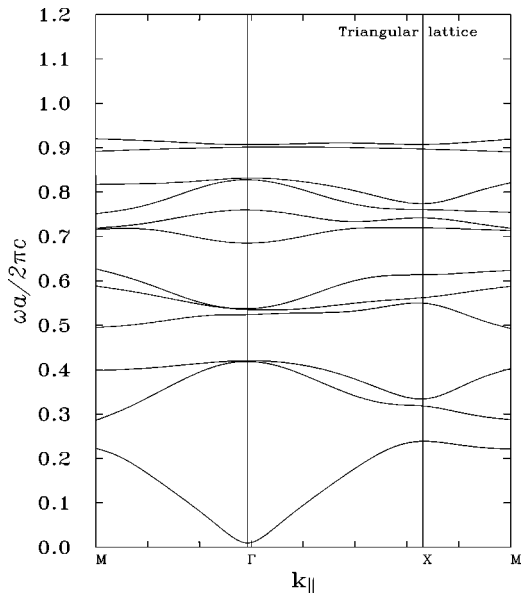

FIG. 4. The photonic band structure for E-polarized electromagnetic (EM) waves in a two-dimensional triangular crystal with the lattice constant $a=1.27$ cm, radius of the rod $R=0.48$ cm, $\epsilon_a=9$, $\epsilon_b=1.04$, and the filling fraction $f=0.518$.

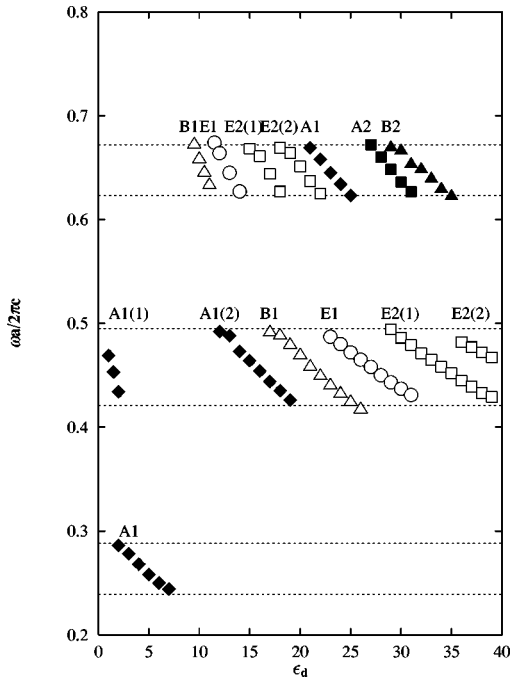

FIG. 5. The eigenfrequencies of localized defect modes belonging to the irreducible representations of the C_{6v} point group as functions of the dielectric constant of the defect cylinder placed in the center of the lattice. The localized modes are depicted within the three lowest frequency band gaps revealed by the photonic band structure shown in Fig. 4. The borders of the gaps are indicated by the horizontal dashed lines. The order of the modes of identical symmetry within the same band is denoted by the number in parentheses.

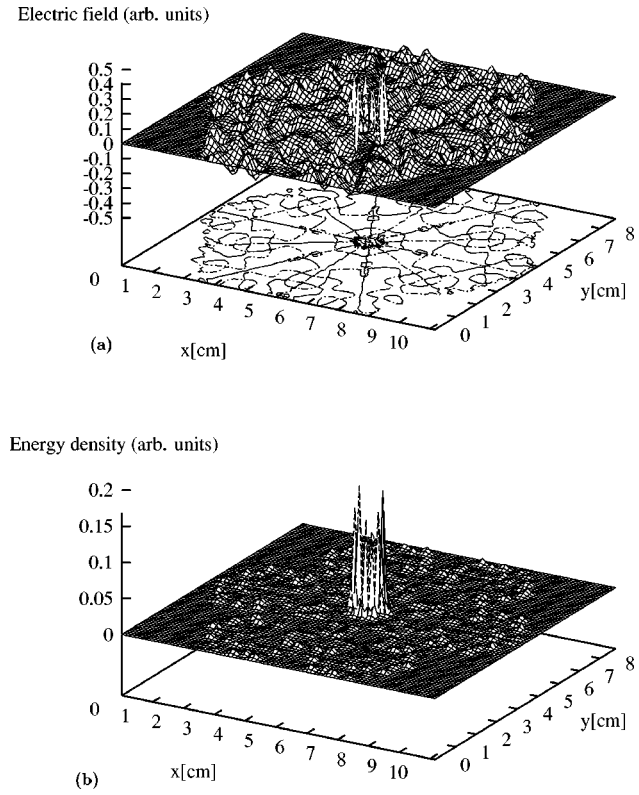

FIG. 6. The spatial distribution (a) of the electric field and (b) the energy density associated with the localized A_2 symmetry defect mode of frequency $\omega a/2\pi c=0.648$ associated with a defect rod with $\epsilon_d=29$. The field patterns are shown within the region of the x_1x_2 plane consisting of 8×8 unit cells.

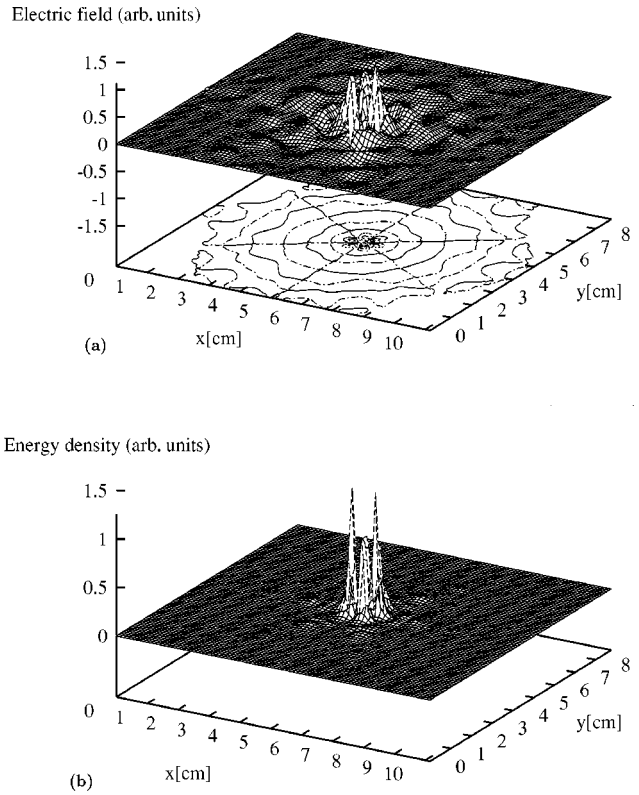

FIG. 7. The spatial distribution (a) of the electric field and (b) the energy density shown in a supercell consisting of 8×8 unit cells associated with the localized B_1 symmetry defect mode of frequency $\omega a/2\pi c=0.469$ associated with the defect rod with $\epsilon_d=20$.

ing periodic boundary conditions. The defect modes investigated within the computational domain are excited by an oscillating dipole centered near the defect cylinder in the photonic crystal, and the solution of Eq. (2.9) is carried out for enough dipole cycles that a converged eigenfrequency and a converged distribution of the electric field associated with the localized mode are achieved.

The symmetry of the eigenmode can be specified by imposing periodic boundary conditions reflecting the characteristics of a particular irreducible representation of the point group C_{6v}, and by placing the dipole in an appropriate symmetrical position. Employing the symmetry of the C_{6v} point group leads to a large reduction of the computational task, since the calculations for the defect modes that correspond to nondegenerate states of A_1, A_2, B_1, and B_2 symmetry were carried out in 1/12 of the supercell, while doubly degenerate states of E symmetry have been calculated within 1/4 of the supercell. By applying all symmetry operations belonging to the C_{6v} point group to the irreducible subdomain we obtained patterns corresponding to each of the individual irreducible representations—shown in Figs. 2(a)–2(e)—where the blank and shaded areas indicate domains that are symmetric and asymmetric, respectively. In Fig. 2(a) we present the configuration consisting of the six nearest-neighboring rods characterized by the dielectric function ϵ_a embedded in the background medium with ϵ_b and with a defect rod in the center of the supercell characterized by ϵ_d. In Fig. 2(a) we also show the mirror reflections $\sigma_{v2},\sigma_{v3},\sigma'_{v1},\sigma'_{v3}$, indicated by broken lines, and σ_{v1},σ'_{v2}, which coincide with the x_1 and x_2 axes, respectively. For the doubly degenerate irreducible representations E_1 and E_2 we display in Fig. 2(e) and Fig. 2(f) the patterns belonging to the E_1^{xz} and E_2^{xy} basis functions. The patterns associated with the partner-basis functions E_1^{yz} and $E_2^{(x^2-y^2)/2}$ belonging to the different rows of identical irreducible representations can be obtained by the rotation of those for E_1^{xz} and E_2^{xy} through $\pi/2$.

The configurations with the defect rod placed in an interstitial position have been calculated within 1/4 of the supercell. In Fig. 3 we display the distributions of subdomains determined by applying of all possible symmetry operations belonging to the C_{2v} point group corresponding to A_1, A_2, B_1, and B_2 symmetry. The blank areas indicate the subdomains that are invariant with respect to the symmetry operations applied to the irreducible subdomain, while the shaded areas correspond to the asymmetric subdomains. In Fig. 3(a) we indicate mirror reflections σ_x,σ_y with respect to the mirror planes that intersect the x_1x_2 plane along the x_1 and x_2-axes, respectively.

III. RESULTS

We first apply the method outlined in the preceding section to the defect modes in a two-dimensional triangular photonic lattice with the lattice constant $a=1.27$ cm, consisting of identical dielectric rods of radius $R=0.48$ cm, which corresponds to the filling fraction $f=0.518$. The cylinders, which are characterized by the dielectric constant $\epsilon_a=9$, are

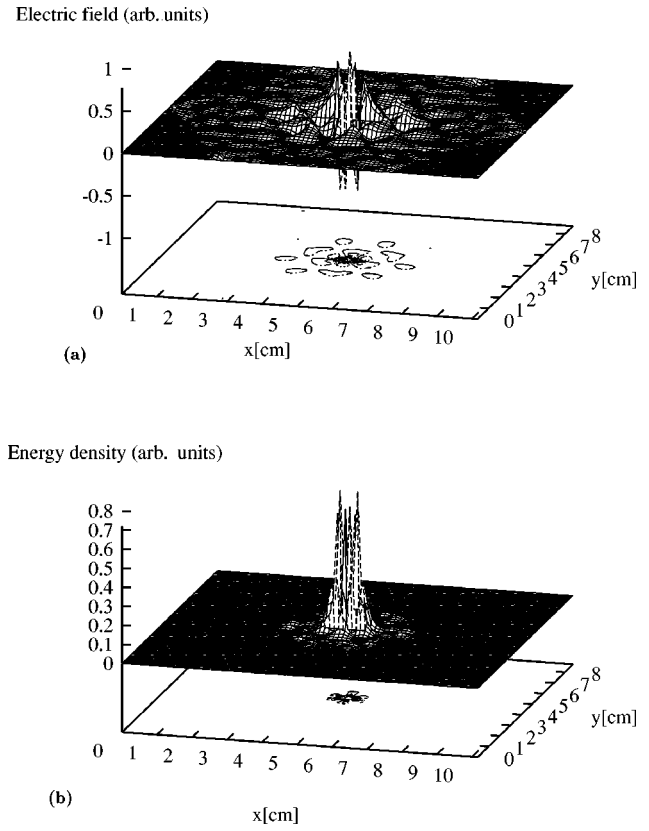

FIG. 8. The spatial distribution (a) of the electric field and (b) the energy density shown in a supercell consisting of 8×8 unit cells associated with the localized B_2 symmetry defect mode of frequency $\omega a/2\pi c=0.63$ associated with a defect rod with $\epsilon_d=36$.

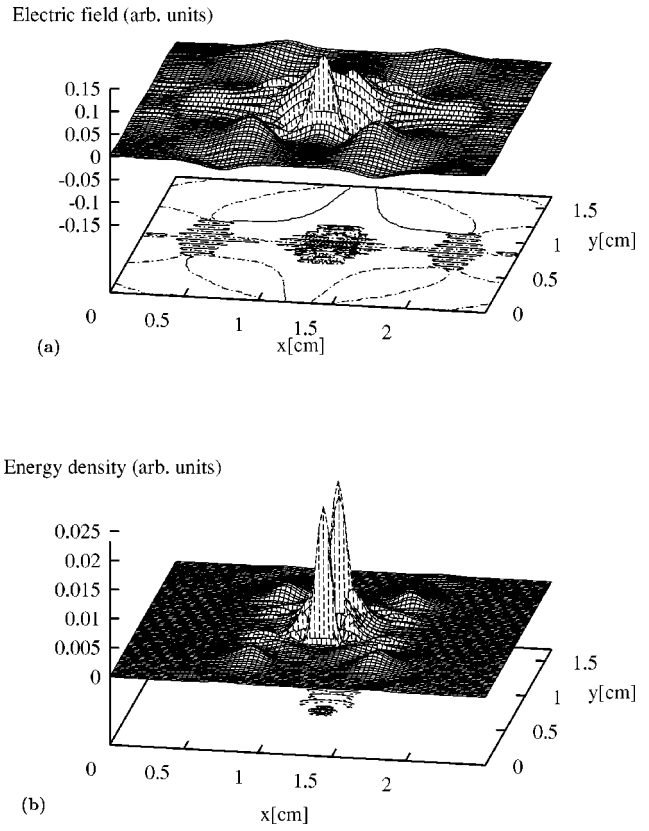

FIG. 9. The spatial distribution (a) of the electric field and (b) the energy density shown in a supercell consisting of 4×4 unit cells associated with the localized E_1 symmetry defect mode of frequency $\omega a/2\pi c=0.472$ associated with a defect rod with $\epsilon_d=24$.

embedded in a background medium with $\epsilon_b=1.04$. This configuration is identical to one of the systems that we considered in our previous paper in which we studied the localized defect modes of A_1 symmetry of the C_{6v} point group.[30] We identified the frequency of the localized defect state created by removing a single rod from the center of the lattice with the sharp peak in the frequency dependence of the transmitted power along the [1,0] direction in the identical system found by Smith *et al.*[12]

In this paper we systematically study the localized defect modes with all symmetries that correspond to the irreducible representations of the C_{6v} point group by varying the dielectric strength of an impurity cylinder placed in the center of the the supercell and in an interstitial position within the triangular lattice. In Fig. 4 we show the photonic band structure for *E*-polarized electromagnetic waves in a two-dimensional triangular crystal with the lattice constant $a=1.27$ cm, and radius of the rod $R=0.48$ cm that corresponds to the filling fraction $f=0.518$. The rods, which are characterized by the dielectric constant $\epsilon_a=9$, are embedded in a background dielectric with the dielectric constant $\epsilon_b=1.04$. The photonic band structure was evaluated by the plane wave method[33] (PWM) by expanding the field variables into 299 plane waves. We are interested in the three lowest frequency band gaps, which in terms of normalized frequencies exist in the regions $0.24<\omega a/2\pi c<0.29$, $0.42<\omega a/2\pi c<0.49$, and $0.62<\omega a/2\pi c<0.68$. For the case of the lattice with the geometrical parameters considered above, the boundaries of the three lowest gaps in GHz are $5.67<\omega<6.86$, $9.93<\omega<11.58$, and $14.66<\omega<16.07$.

By varying the dielectric constant of the impurity cylinder in the range $1<\epsilon_d<40$ and evaluating the frequency dependence of the radiated power of the oscillating dipole placed near the defect rod we have found the localized modes of all symmetries within the three lowest band gaps. Besides the single mode levels of A_1, A_2, B_1, and B_2 symmetry we have found doubly degenerate defect states that reflect the two-dimensional irreducible representations of E_1 and E_2 symmetry. In Fig. 5 we display the dependence of the eigenfrequencies of the localized modes as functions of the dielectric strength of the defect rod. The regions of the three lowest band gaps are denoted by horizontal dashed lines, and the order of the modes of the same symmetry within the same band gap is indicated by the number in the parentheses.

We begin by examining the localized states of A_1 symmetry associated with a configuration with a single rod removed from the center, and gradually increase the dielectric constant of an isolated substitutional rod. We found two sets of localized states of A_1 symmetry that appear at the frequencies close to the upper-band-gap edge when $\epsilon_d=1$ and $\epsilon_d=12$. When we increase ϵ_d the frequencies sweep downwards across the gap to reach the lower edge when $\epsilon_d=2$ and $\epsilon_d=19$, respectively. The third set of resonant modes of A_1 symmetry shown in Fig. 5 appears in the lowest band gap when ϵ_d is in the range $2<\epsilon_d<7$. The localized states of A_2 symmetry appear in the third lowest band when the dielectric constant of the defect ϵ_d is in the range $27<\epsilon_d<31$. In Figs. 6(a) and 6(b) we present the distribution of the electric field

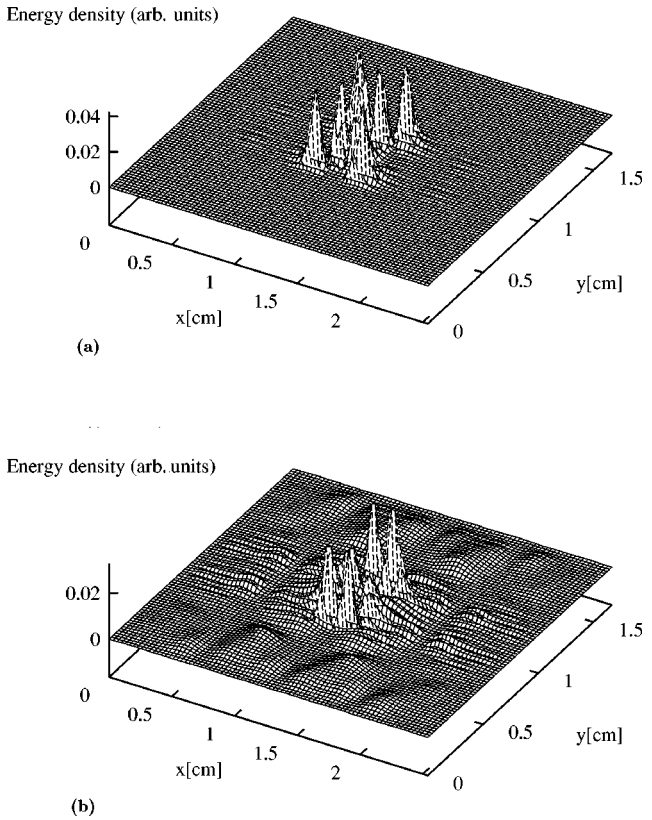

FIG. 10. The spatial distribution the energy density shown in a supercell consisting of 4×4 unit cells associated with the localized modes of E_2 symmetry with frequency (a) $\omega a/2\pi c=0.445$ (b) $\omega a/2\pi c=0.482$ associated with a defect rod characterized by the dielectric constant $\epsilon_d=36$.

and the energy density associated with the defect level of eigenfrequency $\omega a/2\pi c=0.648$ ($\omega=15.32$ GHz). The defect state shown in this figure is associated with an impurity rod with $\epsilon_d=29$. The field patterns are displayed in a region of the x_1x_2 plane consisting of 8×8 unit cells.

Localized states of B_1 symmetry exist in the second and third lowest band gaps. They appear when $17<\epsilon_d<26$ and $9.5<\epsilon_d<11$, respectively. In Figs. 7(a) and 7(b) we show the distribution of the electric field and the energy density associated with the defect mode of B_1 symmetry created by a substitutional impurity rod with $\epsilon_d=20$ and the eigenfrequency $\omega a/2\pi c=0.469$ ($\omega=11.08$ GHz) within the second lowest band. The domain shown in Fig. 7 consists of 8×8 units cells. The localized states of B_2 symmetry appear within the third lowest band gap when $29<\epsilon_d<35$. In Figs. 8(a) and 8(b) we present the distribution of the electric field and the energy density within the supercell consisting of 8×8 unit cells associated with the defect mode due to the substitutional impurity rod with $\epsilon_d=36$ and the eigenfrequency $\omega a/2\pi c=0.63$ ($\omega=14.89$ GHz).

The doubly degenerate localized states of E_1 symmetry that we have found within the second and third lowest band gaps occur for the dielectric constant of the defect rod in the ranges $11.5<\epsilon_d<14$ and $23<\epsilon_d<31$, both of which partially overlap the ranges of ϵ_d in which defect states of B_1 symmetry appear. In Figs. 9(a) and 9(b) we show the distribution of the electric field and the energy density associated

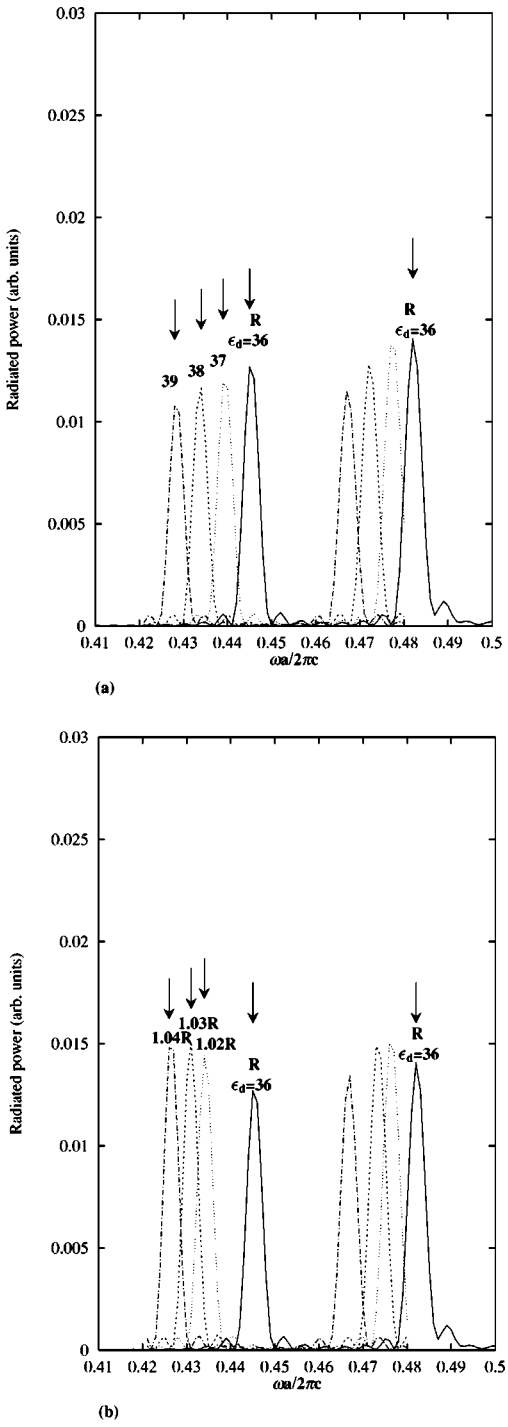

FIG. 11. The electromagnetic energy radiated by an oscillating dipole embedded in a supercell containing a defect (a) with the radius $r_d=R$ when the dielectric strength of the rod is varied in the range $36<\epsilon_d<39$; (b) with the dielectric constant $\epsilon=36$ when the radius of the rod is varied in the range $R<r_d<1.04R$.

with the doubly degenerate defect level with the eigenfrequency $\omega a/2\pi c=0.472$ ($\omega=11.16$ GHz) within the second lowest band gap, which is associated with a defect rod characterized by the dielectric constant $\epsilon_d=24$. We note that the electric-field pattern reflects the symmetry of the E_1^{xz} basis function that is antisymmetric with respect to the C_2 and σ'_{v2} operations of the C_{6v} point group.

The results obtained for the doubly degenerate states of

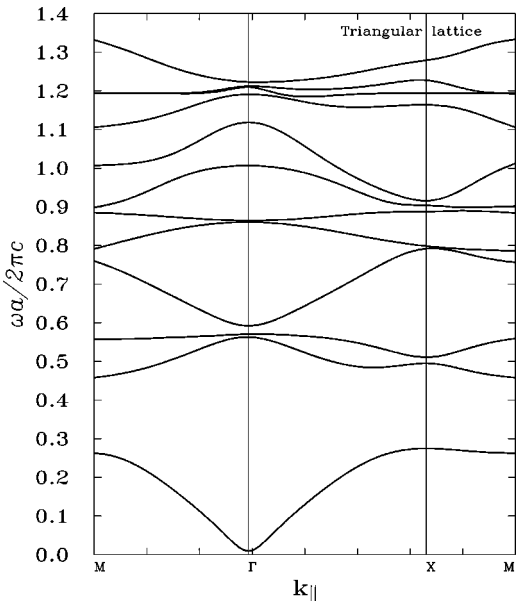

FIG. 12. The photonic band structure for E-polarized EM waves in a two-dimensional triangular crystal with the lattice constant $a=1.27$ cm, radius of the rod $R=0.2a$, $\epsilon_a=13$, $\epsilon_b=1$, and the filling fraction $f=0.145$.

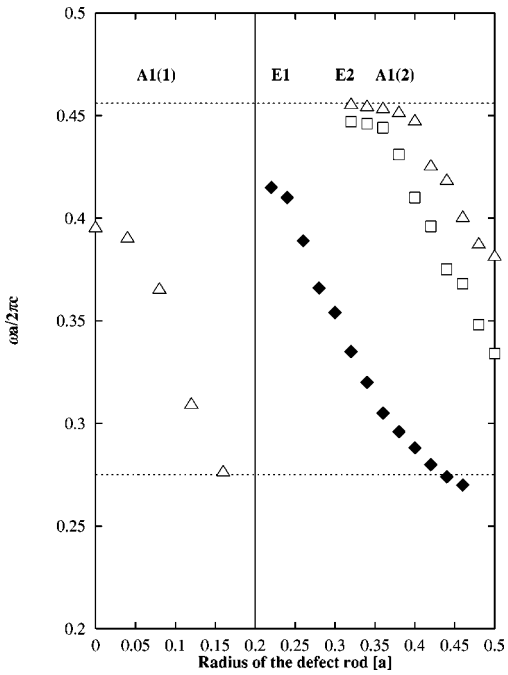

FIG. 13. The eigenfrequencies of localized defect modes belonging to the irreducible representations of the C_{6v} point group as functions of the radius of a defect rod placed in the center of the two-dimensional triangular lattice with the lattice constant $a=1.27$ cm, when $\epsilon_a=13$, $\epsilon_b=1$, $R=0.2a$. The localized modes are shown within the lowest band gap revealed by the photonic band structure shown in Fig. 12 with band edges indicated by the horizontal-dashed lines.

E_2 symmetry reveal the existence of two sets of defect states that appear in the second and the third lowest bands. The defect modes of E_2 symmetry that occur in the second lowest band when $29<\epsilon_d<40$ consist of two levels that coexist for ϵ_d in the range $36<\epsilon_d<39$, and are separated by $\Delta\omega a/2\pi c=0.38$ ($\Delta\omega=0.898$ GHz). The defect modes of E_2 symmetry that appear in the third lowest band and occur when $15<\epsilon_d<22$ also consist of two separate levels that simultaneously appear within this band gap when $\epsilon_d\simeq 18$. In Figs. 10(a) and 10(b) we show the distribution of the energy density associated with the doubly degenerate defect levels with the eigenfrequencies $\omega a/2\pi c=0.445$ ($\omega=10.51$ GHz) and $\omega a/2\pi c=0.482$ ($\omega=11.39$ GHz) within the second lowest band gap, which are associated with a substitutional defect rod characterized by the dielectric constant $\epsilon_d=36$.

In Fig. 11(a) we display the dependence of the radiated power of the oscillating dipole placed in a supercell containing defect rods whose dielectric constant lies in the range $36<\epsilon_d<39$. For each value of the dielectric constant we found two peaks that indicate the existence of doubly degenerate levels of E_2 symmetry, which decrease as ϵ_d increases. The results shown in Fig. 11(b) illustrate an alternative way in which the positions of the eigenfrequencies of the defect modes can be controlled by varying the radius of the rod. For the defect rod characterized by the dielectric constant $\epsilon_d=36$ we have increased the radius of the defect rod in the range $R<r_d<1.04R$. The peaks associated with three different values of the defect radius clearly demonstrate that the frequency of the mode can be tuned downwards to lower frequencies in two equivalent ways—either by increasing the radius or the dielectric strength of the defect rod.

We also examined the system studied by Feng and Arakawa,[21] who considered a two-dimensional triangular photonic crystal with a lattice constant $a=1.27$ cm, consisting of cylinders characterized by the dielectric constant $\epsilon_a=13$ and radius $R=0.2a$ embedded in vacuum. The photonic band structure for E-polarized electromagnetic waves propagating through this lattice, shown in Fig. 12, reveals a photonic band gap in the frequency range $0.275<\omega a/2\pi c<0.46$. Feng and Arakawa, who used a supercell method to study the dependence of the defect levels on defect size, found nondegenerate and doubly degenerate levels that appear when the radius of the defect cylinder is within the range $0<r_d<0.5a$. In our previous paper[30] we have identified a nondegenerate level that appears when the radius is in the range $0.3a<r_d<0.5a$ as possessing A_1 symmetry. By extending the search to all symmetries of the C_{6v} point group we study the dependence of the defect levels on the size of the rod starting from the configuration in which a central rod is completely removed ($r_d=0$). Then we gradually increase the radius of a rod until we reach the close-packed configuration in the vicinity of the defect cylinder ($r_d=0.5a$). In addition to the nondegenerate states that appear in the ranges of the radius of the defect rod $0<r_d<0.18a$ and $0.32a<r_d<0.5a$, which were identified as possessing A_1 symmetry, we have identified the doubly degenerate states that appear when $0.22a<r_d<0.5a$ as those belonging to E_1 and E_2 symmetries. In Fig. 13 we present the dependence of the eigenfrequencies of the localized modes within the lowest band gap in the photonic band structure considered in Ref. 21 on the radius of the defect rod. The boundaries of the gap are indicated by the horizontal dotted lines.

We also studied the possibility of tuning of the defect mode by means of the radial displacement of each of the nearest neighbors of the defect rod. Namely, we examined

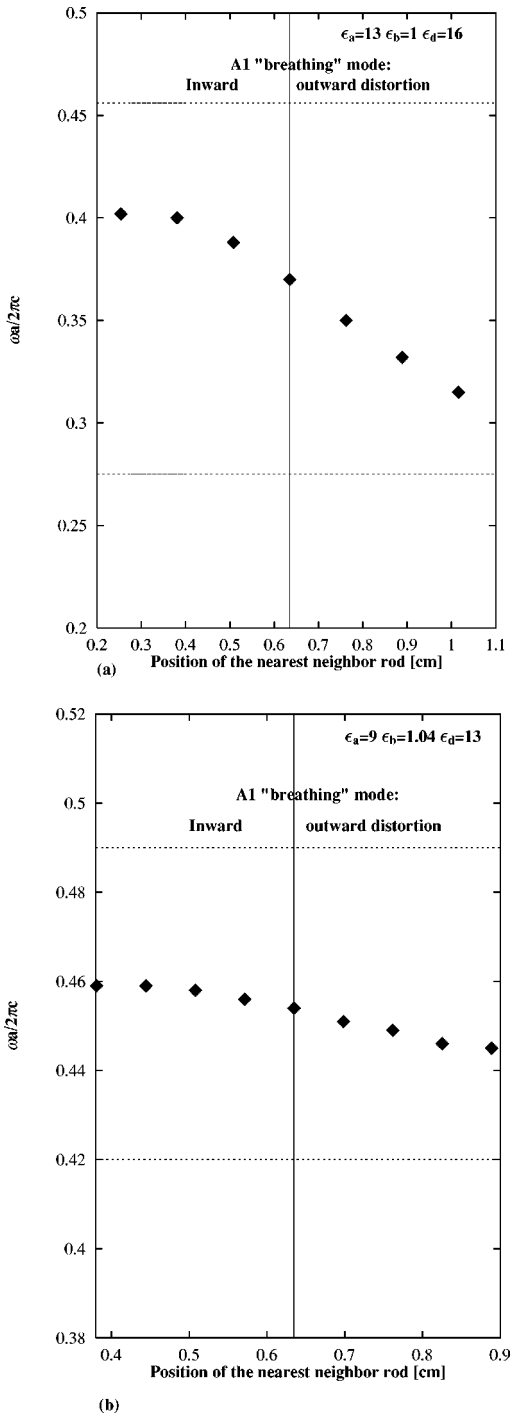

FIG. 14. The effect of a symmetric distortion on the eigenfrequency of the localized mode associated with a substitutional defect rod (a) with $\epsilon_d=13$ embedded in the lattice with $f=0.145$, $\epsilon_a=13$, $\epsilon_b=1$; (b) with $\epsilon_d=16$ embedded in the lattice with $f=0.518$, $\epsilon_a=9$, $\epsilon_b=1.04$.

the effect of the fully symmetric radial displacement of the nearest neighbors, which belongs to the A_1 irreducible representation, on the defect levels produced by a defect rod with the radius $r_d=0.5R$ in the lattice considered in Ref. 21 ($\epsilon_a=13$, $\epsilon_b=1$, $r=0.2a$, $f=0.145$), and on the defect state produced by a defect cylinder characterized by $\epsilon_d=16$ embedded in the lattice considered in Ref. 12. The dependence of both defect levels on the position of the nearest-neighbor rods shown in Figs. 14(a) and 14(b) displays a monotonic

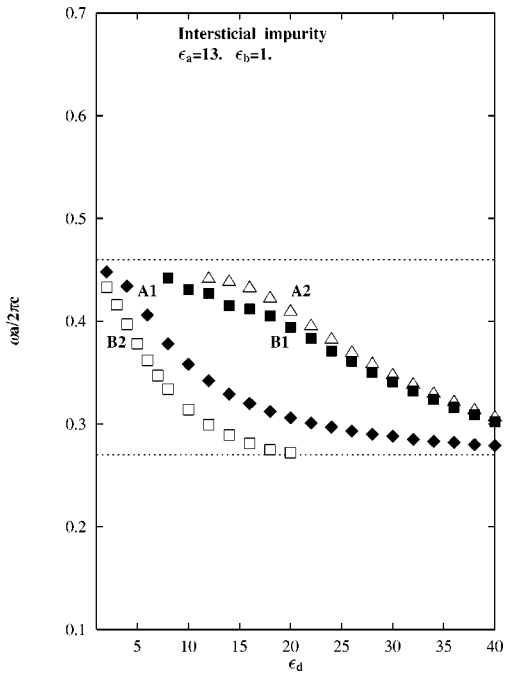

FIG. 15. The eigenfrequencies of localized defect modes belonging to the irreducible representations of the C_{2v} point group as functions of the dielectric constant of two interstitial defect rods placed along the [1,0] direction near the vicinity of the center of the lattice shown in Fig. 3(a). The localized modes are depicted within the lowest frequency band gap revealed by the photonic band structure shown in Fig. 12. The edges of the gaps are indicated by the horizontal-dashed lines.

behavior i.e., the frequency of the modes sweeps upward (downward) across the gap when the inward (outward) distortion of the nearest-neighbor environment occurs.

Now we turn to the results obtained for the defect states implied by a defect consisting of two identical defect rods placed along the [1,0] direction near the cylinder in the center of the supercell that is shown in Fig. 3(a). We again consider the two-dimensional triangular lattice studied in Ref. 21 and concentrate on the *E*-polarized defect modes that appear within the lowest frequency band gap in the frequency range $0.27<\omega a/2\pi c<0.46$. The localized states associated with the two interstitial defects along the [1,0] direction in the hexagonal lattice have been systematically studied by varying the dielectric constant of the defect rods in the range $1<\epsilon_d<40$. By implementing boundary conditions appropriate to the irreducible representations of the C_{2v} point group we have classified the modes of A_1, A_2, B_1, and B_2 symmetry possessing the patterns depicted in Fig. 3(a)–3(d). The values of the eigenfrequencies have been evaluated by solving Eq. (2.9) in 1/4 and 1/2 of the computational domain consisting of 8×8 unit cells.

In Fig. 15 we display the eigenfrequencies of the interstitial defect states of all possible symmetries of the C_{2v} point group as functions of the dielectric strength of the defect cylinder. Here the boundaries of the lowest frequency band gap are indicated by broken lines. The defect modes of B_2 symmetry appear in the band gap as donor states when the dielectric constant $\epsilon_d=2$, and the frequency of the mode sweeps downward across the gap as ϵ_d is increased in the range $2<\epsilon_d<20$. The frequency of the mode of A_1 symme-

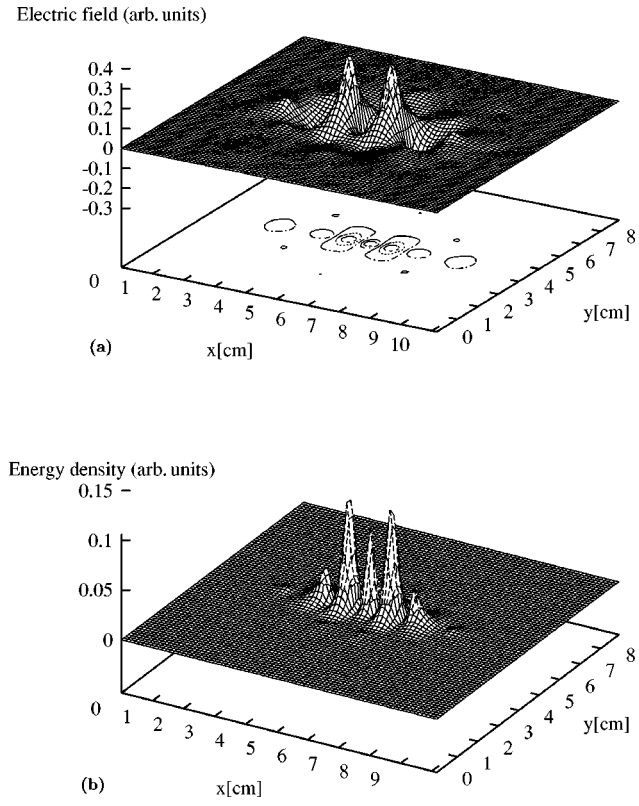

FIG. 16. The spatial distribution (a) of the electric field and (b) the energy density associated with the localized A_1 symmetry defect mode of frequency $\omega a/2\pi c=0.378$ associated with two interstitial defect rods placed along the [1,0] direction with $\epsilon_d=8$. The field patterns are shown within the region of the x_1x_2 plane consisting of 8×8 unit cells.

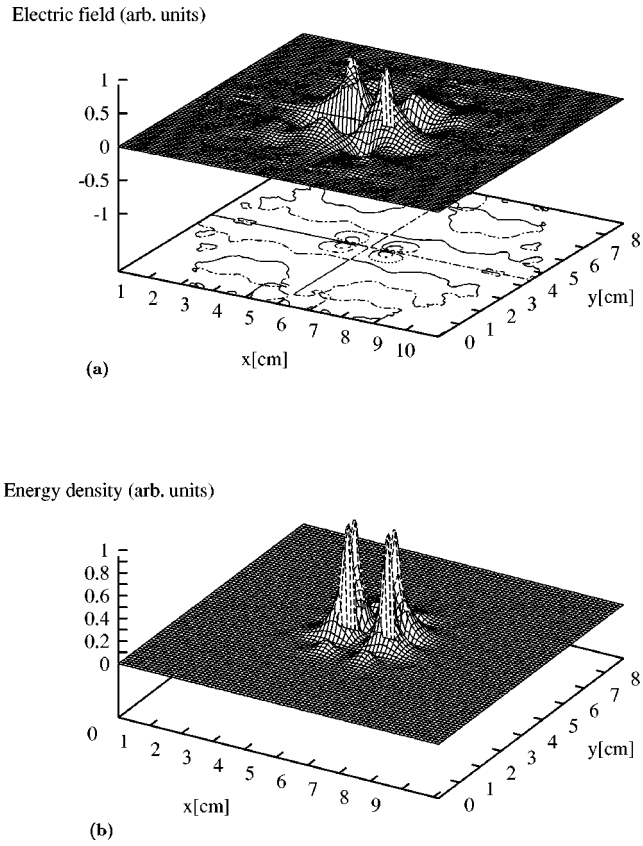

FIG. 17. The spatial distribution (a) of the electric field and (b) the energy density associated with the localized A_2 symmetry defect mode of frequency $\omega a/2\pi c=0.382$ associated with two interstitial defect rods placed along [1,0] direction with $\epsilon_d=24$. The field patterns are shown within the region of the x_1x_2 plane consisting of 8×8 unit cells.

try diplays a similar dependence when the dielectric constant of the defect rod is increased from 2 to 40. Also the defect levels belonging to B_1 and A_2 symmetries, which appear at frequencies close to the upper edge of the band gap when $\epsilon_d=5$ and $\epsilon_d=10$, respectively, decrease monotonically across the band gap when the dielectric constant is increased from 5 to 40.

To demonstrate characteristic features of the field distribution and energy density corresponding to each of the irreducible representations of the C_{2v} point group shown in Fig. 3, we display the electric-field and energy-density patterns associated with (a) an A_1 state with the eigenfrequency $\omega a/2\pi c=0.378$ ($\omega=8.98$ GHz) produced by interstitial rods characterized by $\epsilon_d=8$—see Figs. 16(a) and 16(b); (b) an A_2 state with the eigenfrequency $\omega a/2\pi c=0.382$ ($\omega=9.08$ GHz) that appears when $\epsilon_d=24$—see Figs. 17(a) and 17(b); (c) a B_1 state with the eigenfrequency $\omega a/2\pi c=0.371$ ($\omega=8.82$ GHz) created by the defect rods with $\epsilon_d=24$—see Figs. 18(a) and 18(b); and (d) a B_2 state with the eigenfrequency $\omega a/2\pi c=0.362$ ($\omega=8.61$ GHz) found for the interstitial rods characterized by $\epsilon_d=6$—see Figs. 19(a) and 19(b).

IV. DISCUSSION AND CONCLUSIONS

In this paper we have applied a finite-difference time-domain method to study isolated defects that introduce strongly localized states within the forbidden gaps of a photonic band structure of a two-dimensional photonic lattice that consists of a triangular array of circular dielectric rods. We studied the system with a substitutional rod placed in the center of the supercell, which corresponds to the configuration studied experimentally by Smith *et al.*[12] We also explored the system consisting of two rods placed in interstitial positions along the [1,0] direction in the lattice. By varying the dielectric strength and/or the radius of the defect rods we have studied the dependence of the eigenfrequencies of the defect states on these parameters. The defect levels associated with a substitutional impurity found within the three lowest frequency band gaps possess symmetries corresponding to all the irreducible representations of the C_{6v} point group, while the localized modes induced by defect rods placed in interstitial positions have been found by imposing periodic boundary conditions reflecting the symmetry of each of the irreducible representations of the C_{2v} point group. We found that the doubly degenerate defect states of E_2 symmetry associated with a substitutional defect rod form doublets in certain ranges of the dielectric constant of the defect cylinder. The eigenfrequencies of localized defect modes belonging to the irreducible representations of the C_{2v} point group as functions of the dielectric constant of two interstitial defect rods placed along [1,0] display qualitatively similar behavior as those associated with the substitutional defect rod, except that the localized states of all pos-

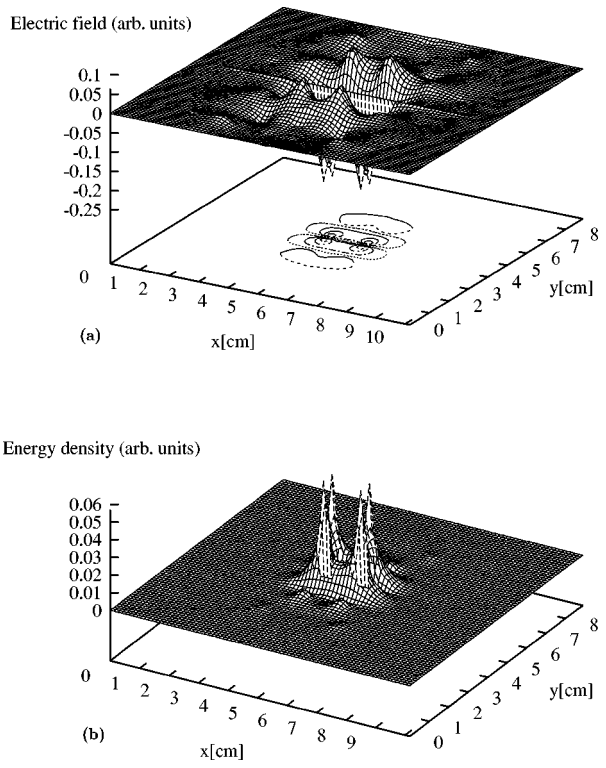

FIG. 18. The spatial distribution (a) of the electric field and (b) the energy density associated with the localized B_1 symmetry defect mode of frequency $\omega a/2\pi c=0.371$ associated with two interstitial defect rods placed along [1,0] direction with $\epsilon_d=24$. The field patterns are shown within the region of the x_1x_2 plane consisting of 8×8 unit cells.

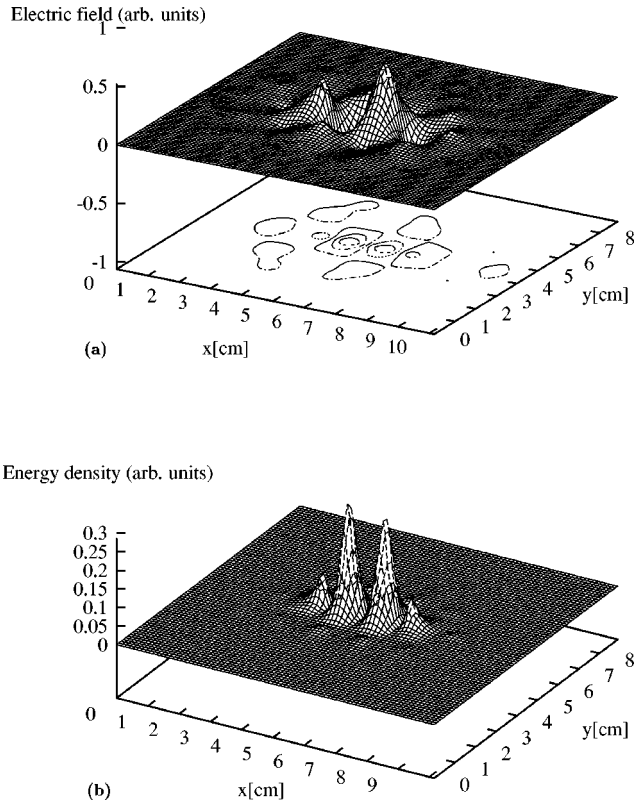

FIG. 19. The spatial distribution (a) of the electric field and (b) the energy density associated with the localized B_2 symmetry defect mode of frequency $\omega a/2\pi c=0.362$ associated with two interstitial defect rods placed along [1,0] direction with $\epsilon_d=6$. The field patterns are shown within the region of the x_1x_2 plane consisting of 8×8 unit cells.

sible symmetries occur simultaneously in a wide range of dielectric strength.

The eigenfrequencies of the modes shown in Fig. 5 and Fig. 15 typically decrease monotonically as ϵ_d is increased. This behavior can be explained in terms of the variational theorem in electromagnetism[4]

$$\omega^2=\frac{\int d\mathbf{r}\frac{1}{\epsilon}|\nabla\times\mathbf{H}|^2}{\int d\mathbf{r}\mathbf{H}^2}, \tag{4.1}$$

which links the mode frequency with the spatial variation of the magnetic-field distribution. First we observe that the eigenfrequency depends on the magnitude of the dielectric strength of the defect rod because it scales as $\omega_d\sim1/\sqrt{\epsilon}$ and, simultaneously, depends on the variation of the field distribution. This, for example, explains the fact that the defect modes with fixed eigenfrequency that belong to the symmetries with a stronger variation of the field distribution occur for larger values of ϵ_d. The variational principle given by Eq. (4.1) also explains the equivalence of adjusting the size of the defect rod and changing the dielectric constant ϵ_d that is demonstrated in Figs. 11(a) and 11(b).

By changing the position of the nearest neighbors in the vicinity of the defect cylinder placed in the center of the supercell we found that symmetric relaxation increases the eigenfrequency of the eigenmode for inward distortion, while the outward distortion leads to a decrease of the defect level. This result can be again interpreted in terms of the variational theorem: the inward distortion increases the average dielectric constant in the region in which most of the variation of the field distribution is concentrated, and this, according to the scaling of the eigenfrequency given by $\omega_d\sim1/\sqrt{\epsilon}$, leads to a lower value of ω_d and vice versa.

We also examined the photonic crystal consisting of GaAs rods arrayed in a two-dimensional triangular lattice considered in Ref. 21, in which the dependence of the frequencies of the localized states on the defect size was studied. By inspecting the defect levels belonging to the irreducible representations of the C_{6v} point group we have identified the nondegenerate and doubly degenerate levels that appear in the band gap for the radius of the defect rod in the range $0<r_d<0.5a$ as those belonging to the A_1, E_1, and E_2 irreducible representations.

The defect size dependence shown in Fig. 13 confirms that the defect produced by reducing the size of the defect rod creates a single acceptorlike defect level that appears close to the lower edge of the band gap, while increasing the radius of the defect rod creates both single and doubly degenerate donorlike levels stemming from the upper edge of the band gap. This is consistent with the results demonstrated theoretically and experimentally in 2D and 3D photonic crystals.[1,5,12]

It is worth pointing out that information on the symmetry provides a natural tool to classify the modes, and belongs along with the eigenfrequency, polarization, and field distri-

bution to the key characteristics that allow identifying peaks observed in transmission measurements. On the other hand, the symmetry analysis of the defect modes plays a crucial role in the coupling efficiency, since incident plane waves can excite only the modes whose symmetry matches the polarization and direction along which the plane wave propagates.

In conclusion, we have systematically studied the defect states associated with substitutional and interstitial defect rods. By imposing boundary conditions appropriate to irreducible representations of the C_{6v} and C_{2v} point groups, and by varying the dielectric strength of the defect rods, we found the defect states associated with all possible irreducible representations. By inspecting the spatial distribution of the electromagnetic field and the energy density we have verified the localized nature of the modes possessing C_{6v} and C_{2v} symmetry. The field distributions of the defect modes resemble the behavior of the basis functions belonging to the irreducible representations. The symmetry analysis allows classifying experimentally observed defect modes and determining the appropriate polarization and direction of propagation of the incident light in order to couple the energy into the cavity. We have shown that the properties of these modes can be controlled by changing the nature and/or the size of the defect. We also studied the effect of a local symmetric distortion of the photonic crystal in the vicinity of the defect rod and interpreted the results obtained by using the variational theorem. Studies in progress focus on the extension of the present method to the solution of the problem of surface modes and to frequency-dependent and nonlinear Kerr-like defects. We also plan to study energy transfer between interacting defects and other properties associated with the temporal behavior of the modes.

ACKNOWLEDGMENTS

The work of V.K. was supported by NSF Grant No. INT-932651 and in part by COST 268 Action. The work of A.A.M. was supported in part by NSF Grant No. DMR-9319404.

*Permanent address: Institute of Radio Engineering and Electronics, Czech Academy of Sciences, Chaberska 57, 182 51 Prague 8, Czech Republic.

[1] E. Yablonovitch, Phys. Rev. Lett. **58**, 2486 (1987).

[2] S. John, Phys. Rev. Lett. **58**, 2059 (1987).

[3] For recent reviews see the articles in *Photonic Band Gaps and Localization*, edited by C. M. Soukoulis (Plenum, New York, 1993); J. Opt. Soc. Am. B **10** (1993), special issue on Development and Applications of Materials Exhibiting Photonic Band Gaps, edited by C. M. Bowden, J. P. Dowling, and H. O. Everitt; J. Mod. Opt. **41** (1994), special issue on Confined Electrons and Photons, edited by E. Burstein and C. Weisbuch, Vol. 340 of *NATO Advanced Studies Institute, Series B: Physics*, edited by E. Burstein and C. Weisbuch (Plenum, New York, 1995); in *Photonic Band Gap Materials*, Vol. 315 *NATO Advanced Studies Institute, Series E: Applied Sciences*, edited by C. M Soukoulis (Kluwer, Dordrecht, 1996); and in *Microcavities and Photonic Bandgaps: Physics and Applications*, Vol. 324 of *NATO Advanced Studies Institute, Series E: Physics*, edited by J. Rarity and C. Weisbuch (Kluwer, Dordrecht, 1996).

[4] J. D. Joannopoulos, R. D. Meade, and J. N. Winn, *Photonic Crystals, Molding the Flow of Light* (Princeton University Press, Princeton, NJ, 1995).

[5] S. L. McCall, P. M. Platzman, R. Dalichaouch, D. Smith, and S. Schultz, Phys. Rev. Lett. **67**, 2017 (1991).

[6] R. Dalichaouch, J. P. Armstrong, S. Schultz, P. M. Platzman, and S. L. McCall, Nature (London) **354**, 53 (1991).

[7] W. Robertson, G. Arjavalingam, R. D. Meade, K. D. Brommer, A. M. Rappe, and J. D. Joannopoulos, Phys. Rev. Lett. **68**, 2023 (1992).

[8] E. Yablonovitch, T. J. Gmitter, R. D. Meade, A. M. Rappe, K. D. Brommer, and J. D. Joannopoulos, Phys. Rev. Lett. **67**, 3380 (1991).

[9] E. Yablonovitch, J. Opt. Soc. Am. B **10**, 283 (1993).

[10] R. D. Meade, K. D. Brommer, A. M. Rappe, and J. D. Joannopoulos, Phys. Rev. B **44**, 13 772 (1991).

[11] R. D. Meade, K. D. Brommer, A. M. Rappe, and J. D. Joannopoulos, Phys. Rev. B **48**, 8434 (1993).

[12] D. R. Smith, R. Dalichaouch, N. Kroll, S. Schultz, S. L. McCall, and P. M. Platzman, J. Opt. Soc. Am. B **10**, 314 (1993).

[13] D. R. Smith, N. Kroll, and S. Schultz, in *Photonic Band Gap Materials*, edited by C. M Soukoulis (Kluwer, Dordrecht, 1996), p. 391.

[14] K. M. Leung, J. Opt. Soc. Am. B **10**, 303 (1993).

[15] A. A. Maradudin and A. R. McGurn, in *Photonic Band Gaps and Localization*, edited by C. M Soukoulis (Plenum, New York, 1993), p. 247.

[16] M. Sigalas, C. M. Soukoulis, E. N. Economou, and C. T. Chan, Phys. Rev. B **48**, 14 121 (1993).

[17] M. Sigalas, C. M. Soukoulis, C. T. Chan, and K. M. Ho, Phys. Rev. B **49**, 11 080 (1994).

[18] A. R. McGurn and M. Khazhinsky, in *Photonic Band Gap Materials*, edited by C. M Soukoulis (Kluwer, Dordrecht,1996), p. 487.

[19] E. Yablonovitch and D. E. Sievenpiper, Phys. Rev. Lett. **76**, 2480 (1996).

[20] C. T. Chan, Q. L. Yu, and K. M. Ho, Phys. Rev. B **51**, 16 635 (1995).

[21] X.-P. Feng and Y. Arakawa, Jpn. J. Appl. Phys., Part 2 **36**, L122 (1997).

[22] S. John and J. Wang, Phys. Rev. B **43**, 12 722 (1991).

[23] S. Fan, P. Villeneuve, and J. D. Joannopoulos, Phys. Rev. B **54**, 11 245 (1996).

[24] J. N. Winn, S. Fan, and J. D. Joannopoulos, Phys. Rev. B **59**, 1551 (1999).

[25] J. B. Pendry and A. Mackinnon, Phys. Rev. Lett. **69**, 2772 (1992).

[26] T. Nakayama, K. Yakubo, and R. L. Orbach, Rev. Mod. Phys. **66**, 381 (1994).

[27] T. Nakayama, K. Yakubo, and M. Takano, Phys. Rev. B **47**, 9249 (1993).

[28] K. Sakoda and K. Ohtaka, Phys. Rev. B **54**, 5732 (1996).

[29] K. Sakoda and H. Shiroma, Phys. Rev. B **56**, 4830 (1997).

[30] V. Kuzmiak and A. A. Maradudin, Phys. Rev. B **57**, 15 242 (1998).

[31] K. Sakoda, T. Ueta, and K. Ohtaka, Phys. Rev. B **56**, 14 905 (1997).

[32] P. R. Villeneuve and M. Piché, Phys. Rev. B **46**, 4969 (1992).

[33] M. Plihal and A. A. Maradudin, Phys. Rev. B **44**, 8565 (1991).